Carrier-Based Modulation Strategies With Reduced Common-Mode Voltage for Five-Phase Voltage Source Inverters

Wenjing Xiong, Yao Sun, *Member, IEEE*, Mei Su, Jianxin Zhang, Yonglu Liu, and Jian Yang, *Member, IEEE*

***Abstract*—Two modulation strategies based on carrier-based modulation (CBM) scheme (named RCMV-CBM1 and RCMV-CBM2) are proposed to reduce the common-mode voltage (CMV) of a five-phase voltage source inverter. The basic characteristic of them is that two kinds of carriers with opposite phase are adopted. By applying the opposite carrier to some specific phases, the switching states with higher CMV absolute value can be avoided. In RCMV-CBM1, the output phase with the third largest modulated signal uses the opposite carrier, and the peak-to-peak value of CMV is reduced by 40%. In RCMV-CBM2, the output phases with the second largest and fourth largest modulated signals use the opposite carrier, and the peak-to-peak value of CMV is decreased by 80%. However, the ripple analysis reveals that RCMV-CBM1 has an advantage over RCMV-CBM2 in current quality. In addition, the optimized RCMV-CBM1 and RCMV-CBM2 are presented for reducing the output current ripple. Finally, a scaled-down prototype is built to verify the correctness and effectiveness of the proposed modulation strategies.**

***Index Terms*—Carrier-based modulation (CBM), common-mode voltage (CMV), five-phase voltage source inverter (VSI).**

I. Introduction

COMMON-MODE voltage (CMV) widely exists in typical power inverters. It will stimulate the distributed and parasitic capacitances in the system and thus results in common-mode current. In inverter-driven induction motor systems, the common-mode current will produce shaft voltages and bearing currents [1]. The overload bearing current would speed up the aging of the motor bearing and shorten the service life of the motor [2], [3]. Additionally, the CMV can also cause electromagnetic interference (EMI) [4]. Therefore, it is necessary to reduce the CMV in inverters.

Manuscript received November 4, 2016; revised January 9, 2017 and February 23, 2017; accepted April 2, 2017. Date of publication April 12, 2017; date of current version December 1, 2017. This work was supported in part by the National Natural Science Foundation of China under Grants 61573382 and 61622311, in part by the Natural Science Foundation of Hunan Province, China, under Grant 2016JJ1019, and in part by the Project of Innovation-Driven Plan in the Central South University, and in part by the Program for New Century Excellent Talents in University under Grant NCET-13-0599. Recommended for publication by Associate Editor Brendan P. McGrath. *(Corresponding author: Yao Sun.)*

The authors are with the School of Information Science and Engineering, Central South University, Changsha 410083, China (e-mail: csu.xiong@163.com; yaosuncsu@gmail.com; sumeicsu@mail.csu.edu.cn; 2665376@163.com; liuyonglu@csu.edu.cn; fish2bear@gmail.com).

Color versions of one or more of the figures in this paper are available online at http://ieeexplore.ieee.org.

Digital Object Identifier 10.1109/TPEL.2017.2692778

A large number of solutions have been proposed to address the aforementioned issue, and they can be roughly classified into hardware and software methods. The hardware method mainly includes EMI filter redesign and circuit topology modification [4]–[10], while the software one is realized by developing proper modulation strategies with reduced CMV [11]–[27]. Generally, the latter is preferable as it will not increase the cost, weight, and size of the inverters.

Carrier-based modulation (CBM) and space vector modulation (SVM) are two commonly used pulse width modulation (PWM) modulation techniques. Most modulation methods with the reduced CMV are based on the frameworks of them. The basic idea to reduce CMV is to avoid using the switching states with a high CMV in the design of modulation strategies. In [11], an SVM method is proposed to reduce the CMV of two-level three-phase voltage source inverter (VSI), in which zero vectors are replaced by two active space vectors in the opposite phase. The SVM method using three adjacent active vectors to synthesize the desired voltage vector is presented in [12], which has reduced switching losses but smaller linear modulation range. By combining the methods in [11] and [12], a high-performance SVM method is presented in [13]. In addition, three space vectors with a phase shift of 120° to each other are adopted to reduce the CMV in [14], but the maximum modulation index is limited to 0.667. In [15], a novel random SVM method is proposed for the CMV reduction of a two-level three-phase VSI. In [16] and [17], the SVM methods using the vectors with zero CMV are proposed for the multilevel inverters with odd number of levels. In this case, perfect zero CMV can be achieved. A CBM method presented in [18] and [21] can effectively reduce the CMV of the two-level three-phase VSI. The basic idea behind this method is applying the opposite carrier to the output phase with the second largest modulated signal value. The phase-shifted CBM method (PS-CBM) [22]–[24], using three carriers with a phase difference of one-third of the carrier period, could reduce the probability of appearing zero switching state greatly. However, the peak-to-peak value of CMV cannot be reduced when the modulation index is higher than 0.667. A scheme of carrier peak position CBM method is presented in [9], [25], and [26]. It is performed by delaying or advancing the position of triangular carriers to avoid the zero switching states, so the peak-to-peak value of CMV is reduced in the whole range of the modulation index (0–1.1547). For multilevel VSI,

the PS-CBM method and phase disposition CBM method are adopted to reduce the CMV [27]. In addition, a CBM method with zero CMV is proposed for a three-level VSI, in which two modulation signals with a phase angle of 120° are utilized for each output phase [17]. Actually, by selecting zero-sequence components and carrier patterns properly, the CBM methods are equivalent to the corresponding SVM methods [28], [29].

Nowadays, the multiphase induction motors (mainly refer to the motor whose phase number is greater than three in this paper) have attracted much attention, because they have many advantages over three-phase motors, such as better fault tolerance capability, lower power rating in each bridge arm by splitting the motor current across a higher number of phases, higher torque density by current harmonic injection [30]–[33]. Thus, they could be applied in electric vehicles, marine electric propulsion, and high power applications [32], [33]. The most commonly used converter for multiphase applications is the two-level multiphase VSI, where the CMV is also a critical issue. However, there are few literature addressing the CMV issue in the multiphase VSI. In [34]–[39], the CBM methods and SVM methods are tailored for the multiphase VSI without considering the CMV issue. In [40], a finite-set model predictive control (MPC) technique is used to mitigate the CMV of a five-phase VSI. In [41], the PS-CBM method is utilized for multiphase inverters, and the zero CMV is achieved when the output phase number of the inverter is even. For the inverter with odd output phase number, taking the five-phase VSI as an example, the PS-CBM reduces the maximum peak-to-peak value of CMV by 80% at low modulation index and 40% at high modulation index. An SVM method adopting six adjacent large space vectors is presented for a five-phase VSI [42], [43], in which the peak-to-peak value of the CMV is reduced to $0.2V_{\rm dc}$. In [44], an SVM method with zero CMV is proposed for an open-end winding five-phase VSI, but the modulation range gets smaller.

With the increase of the phase number of VSI, the implementation of SVM methods will be very complicated. Therefore, the CBM methods become more attractive in the multiphase VSI. This paper proposes two CBM methods to reduce the CMV for a five-phase VSI, which are named as RCMV-CBM1 and RCMV-CBM2 for short. It is worth noting that the maximum linear modulation index keeps unchanged under the proposed strategies. Inspired by the work of the two-level three-phase VSI in [19], two carriers with opposite phase are employed for the proposed methods. The key point is to decide which phases use the opposite carrier. Different selections lead to different modulation strategies, and it will show different performance. In RCMV-CBM1, the opposite carrier is used in the output phase with the third largest modulated signals value. As a result, the peak-to-peak value of CMV is decreased by 40%. In RCMV-CBM2, the opposite carrier is applied to two output phases which have the second largest and fourth largest modulated signal values, and then the peak-to-peak value of CMV is further decreased by 80%.

The remainder of this paper is organized as follows: Section II introduces the topology structure and the CMV analysis of the five-phase VSI. In Section III, the generalized CBM scheme and two kinds of CMV reduction modulation strategies: RCMV-CBM1 and RCMV-CBM2 are demonstrated. In Section IV, the current quality comparison of three CBM methods and the optimized CBM methods for reducing the current ripple are presented. The comparisons between RCMV-CBM2 and other CMV reduced methods are provided in Section V. In Section VI, the experimental results are illustrated, and finally, Section VII summarizes the major contributions of this work and discusses ideas for future work.

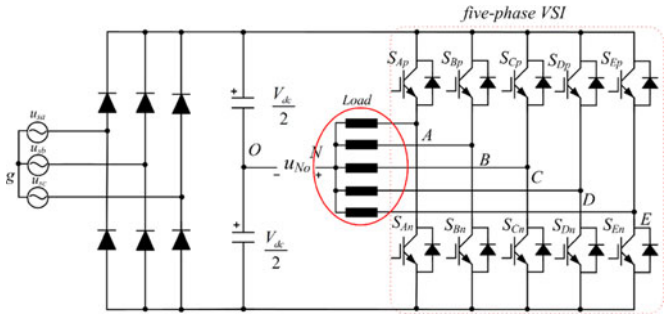

Fig. 1. Topology of a five-phase VSI.

TABLE I
COMMON-MODE VOLTAGE OF A FIVE-PHASE VSI

Group	Switching state combinations $(S_{\rm Ap}S_{\rm Bp}S_{\rm Cp}S_{\rm Dp}S_{\rm Ep})$	$\lvert u_{\rm No}\rvert$
1	(00000) (11111)	$0.5V_{\rm dc}$
2	(10000)(01000)(00100)(00010)(00001) (01111)(10111)(11011)(11101)(11110)	$0.3V_{\rm dc}$
3	(11000)(10100)(10010)(10001)(01100) (01010)(01001)(00110)(00101)(00011) (00111)(01011)(01101)(01110)(10011) (10101)(10110)(11001)(11010)(11100)	$0.1V_{\rm dc}$

II. CMV ANALYSIS FOR A FIVE-PHASE VSI

The circuit topology of a five-phase VSI is shown in Fig. 1. Its CMV is defined as the voltage between load neutral point "*N*" and the midpoint of dc power supply "*O*," which can be described as follows:

$$u_{\rm No}=\frac{u_{\rm Ao}+u_{\rm Bo}+u_{\rm Co}+u_{\rm Do}+u_{\rm Eo}}{5} \tag{1}$$

where

$$u_{\rm io}=(S_{\rm ip}-S_{\rm in})\frac{V_{\rm dc}}{2}, i\in\{A,B,C,D,E\}. \tag{2}$$

Then, the CMV can be further expressed as

$$u_{\rm No}=\frac{\sum_{i=A,B,C,D,E}(S_{\rm ip}-S_{\rm in})V_{\rm dc}}{10} \tag{3}$$

where $S_{\rm ip}$ and $S_{\rm in}$ denote the states of respective switches, "1" means ON-state, and "0" means OFF-state.

The CMV absolute values of the five-phase VSI of all switching states are illustrated in Table I, which can be classified into three groups. In group 1, all the five upper switches or lower switches are ON. The switching states have the largest CMV and

are referred to as zero states [35]. In group 2, one or four upper switches are ON. The corresponding switching states lead to the second largest CMV and are referred to as medium vectors. In group 3, two or three upper switches are ON. Clearly the CMV absolute values in group 3 are the smallest. It is easy to find that a reduced CMV can be achieved by discarding the switching states in group 1 and group 2, especially group 1.

III. Proposed Carrier-Based Modulation Scheme

A. Generalized CBM Method

Assume that the desired output phase voltages are

$$\begin{cases} u^*_{\mathrm{AN}} = U_{\mathrm{om}} \cos(\omega t) \\ u^*_{\mathrm{BN}} = U_{\mathrm{om}} \cos\left(\omega t - \dfrac{2\pi}{5}\right) \\ u^*_{\mathrm{CN}} = U_{\mathrm{om}} \cos\left(\omega t - \dfrac{4\pi}{5}\right) \\ u^*_{\mathrm{DN}} = U_{\mathrm{om}} \cos\left(\omega t - \dfrac{6\pi}{5}\right) \\ u^*_{\mathrm{EN}} = U_{\mathrm{om}} \cos\left(\omega t - \dfrac{8\pi}{5}\right) \end{cases} \tag{4}$$

where U_{om} and ω are the amplitude and angular frequency of the output voltages, respectively.

The modulated signals are expressed as

$$u^*_{\mathrm{io}} = u^*_{\mathrm{in}} + u_{\mathrm{no}},\ i \in \{A, B, C, D, E\} \tag{5}$$

where u^*_{io} is the modulated signal, and u_{no} denotes the zero-sequence signal.

To maximize dc voltage utilization ratio, a proper zero-sequence signal should be determined carefully.

From (4) and (5), the range of the zero-sequence signal u_{no} is

$$-\frac{V_{\mathrm{dc}}}{2} - u_{\min} \le u_{\mathrm{no}} \le \frac{V_{\mathrm{dc}}}{2} - u_{\max} \tag{6}$$

where $u_{\min} = \min(u^*_{\mathrm{AN}}, \ldots, u^*_{\mathrm{EN}})$, $u_{\max} = \max(u^*_{\mathrm{AN}}, \ldots, u^*_{\mathrm{EN}})$.

Equivalently, u_{no} can be further expressed as follows:

$$u_{\mathrm{no}} = \frac{(1-2\lambda)V_{\mathrm{dc}} - \lambda u_{\min} - (1-\lambda)u_{\max}}{2},\ \lambda \in [0,1]. \tag{7}$$

In the case of $\lambda = 0$ or 1, the corresponding modulation schemes are referred to as the discontinuous PWM algorithm. When $\lambda = 0.5$, it is called as the standard CBM [11].

For convenience, the modulated signals are normalized as

$$\bar{u}_{\mathrm{io}} = \frac{u^*_{\mathrm{io}}}{V_{\mathrm{dc}}/2}. \tag{8}$$

Then, they satisfy the following constraints:

$$-1 \le \bar{u}_{\mathrm{io}} \le 1. \tag{9}$$

Usually, the modulation index *M* is defined as

$$M = \frac{U_{\mathrm{om}}}{V_{\mathrm{dc}}/2}. \tag{10}$$

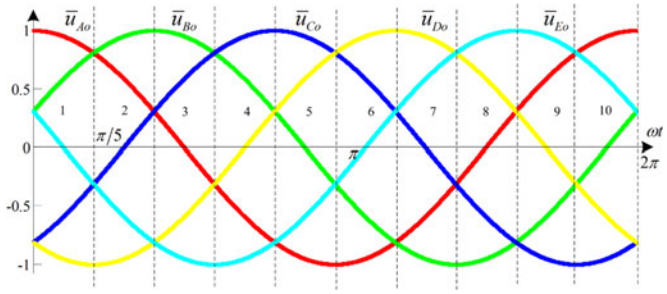

Fig. 2. Relationship of five desired output voltages.

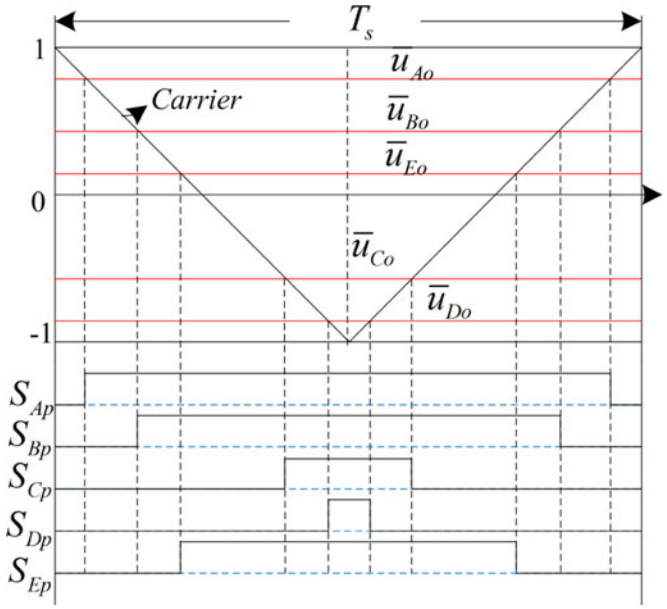

Fig. 3. Schematic diagrams and related switching patterns of generalized CBM.

By injecting the zero sequence signal to the modulated signals, the maximum modulation index can increase beyond unity. According to (6), the maximum linear modulation index of the five-phase VSI [45] is

$$M_{\max} = \frac{1}{\cos\left(\frac{\pi}{10}\right)} = 1.0515. \tag{11}$$

Clearly, the value order of five modulated signals will keep unchanged no matter which zero sequence signal is injected. Therefore, to show the value relationship of five output voltages, the modulated signals without injecting the zero sequence signal are plotted in Fig. 2. Assume the modulated signals keep unchanged in a modulation period *Ts* and the desired output voltages are in sector 1 (refer to Fig. 2). When an isosceles triangle carrier signal is used, the corresponding switching patterns in a modulation period *Ts* are shown in Fig. 3. As seen, the pulse pattern of S_{ip} is 0-1-0. There are six switching state combinations, i.e., (00000), (10000), (11000), (11001), (11101), and (11111). It can be concluded that under the generalized CBM, the switching states in group1 will always exist. From the perspective of reducing CMV, such a modulation scheme is undesired.

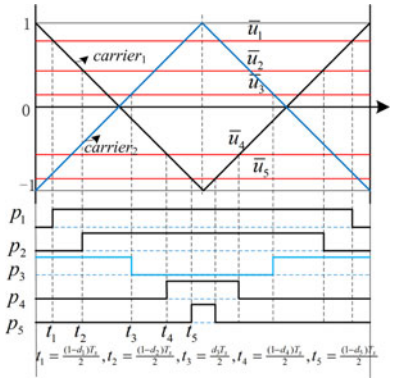

Fig. 4. Schematic diagrams and related switching patterns of RCMV-CBM1.

B. RCMV-CBM1

In CBM, the ways to change switching patterns include modifying the modulated signals and the shapes of carrier waves. However, modifying the modulated signals cannot eliminate the switching states (00000) and (11111) simultaneously. Thus, the way to change the shapes of carrier is used. In this section, an opposite carrier is used in a specific phase.

To facilitate analysis, we sort the desired output voltages u_{in}^* from high to low, and denote them as $u_1^* \geq u_2^* \geq u_3^* \geq u_4^* \geq u_5^*$. Meanwhile, denote the corresponding five output phases as p_1, p_2, p_3, p_4, and p_5, respectively.

The proposed RCMV-CBM1 is illustrated in Fig. 4, where carrier$_2$ is in opposite phase with carrier$_1$. The characteristic of RCMV-CBM1 is that phase-p_3 uses carrier$_2$, and the remaining phases use carrier$_1$.

As seen, to eliminate the switching states (00000) and (11111), the following constraints should be satisfied:

$$t_1 \leq t_3 \leq t_5 \tag{12}$$

where $t_1 = \frac{(1-d_1)T_s}{2}$, $t_3 = \frac{d_3 T_s}{2}$, $t_5 = \frac{(1-d_5)T_s}{2}$, and d_j $(j = 1, 2, 3, 4, 5)$ is the duty cycle of the upper switch of phase-p_j over a modulation period, and it can be expressed as

$$d_j = \frac{1}{2} + \frac{\left(u_j^* + u_{\text{no}}\right)}{V_{\text{dc}}}. \tag{13}$$

From (5)–(8), (12), and (13), the range of u_{no} can be derived as

$$\max\left(\frac{-u_1^* - u_3^*}{2}, -\frac{V_{\text{dc}}}{2} - u_5^*\right) \leq u_{\text{no}} \leq \min\left(\frac{-u_5^* - u_3^*}{2}, \frac{V_{\text{dc}}}{2} - u_1^*\right). \tag{14}$$

The range of $\bar{u}_{\text{no}}$ ($\bar{u}_{\text{no}} = \frac{u_{\text{no}}}{V_{\text{dc}}/2}$) [refer to (14)], when the desired five-phase output voltages are balanced and sinusoidal, and $M \leq 1.0515$, is illustrated in Fig. 5. The two surfaces shown in Fig. 5 stand for the upper and lower boundaries of $\bar{u}_{\text{no}}$ at different instants and M. As seen, the upper boundary is always higher than the lower boundary, which means that there is always a feasible u_{no}. Meanwhile, the range of the feasible solution is relatively narrow when M is close to 1.0515.

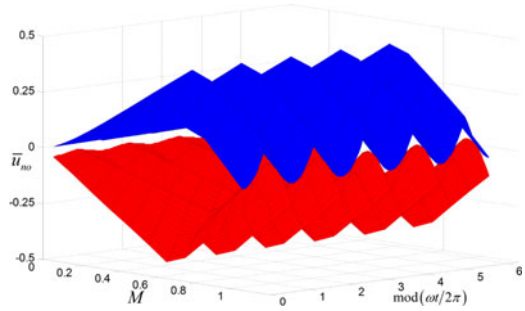

Fig. 5. Range of u_{no} based on RCMV-CBM1.

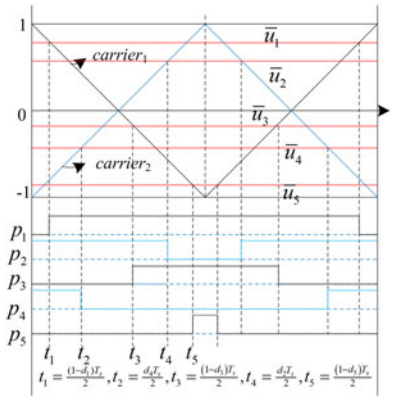

Fig. 6. Schematic diagrams and related switching patterns of RCMV-CBM2.

C. RCMV-CBM2

Based on the analysis in Section II, if only the switching states in group 3 are adopted, the peak-to-peak value of CMV will be further reduced to 0.2 V_{dc}. To this end, an intuitive way is that the opposite carrier is used in more phases.

In this section, RCMV-CBM2 is proposed, and its schematic diagram is shown in Fig. 6. The opposite carrier is applied in phases p_2 and p_4. To ensure that only the switching states in group 3 are used, the following constraints must be met:

$$t_1 \leq t_2 \leq t_3 \leq t_4 \leq t_5 \tag{15}$$

where

$$t_1 = \frac{(1-d_1)T_s}{2},\ t_2 = \frac{d_4 T_s}{2},\ t_3 = \frac{(1-d_3)T_s}{2},$$
$$t_4 = \frac{d_2 T_s}{2},\ t_5 = \frac{(1-d_5)T_s}{2}.$$

Substituting (13) and (5)–(8) into (15), it yields

$$l_1 \leq u_{\text{no}} \leq l_2 \tag{16}$$

where

$$\begin{cases} l_1 = \max\left(-\frac{V_{\text{dc}}}{2} - u_5^*, \frac{-u_1^* - u_4^*}{2}, \frac{-u_3^* - u_2^*}{2}\right) \\ l_2 = \min\left(\frac{V_{\text{dc}}}{2} - u_1^*, \frac{-u_3^* - u_4^*}{2}, \frac{-u_5^* - u_2^*}{2}\right) \end{cases}. \tag{17}$$

Under the assumption in (4), it can be deduced that $l_1 \leq l_2$ is always established at any instants when $M \leq 1.0515$.

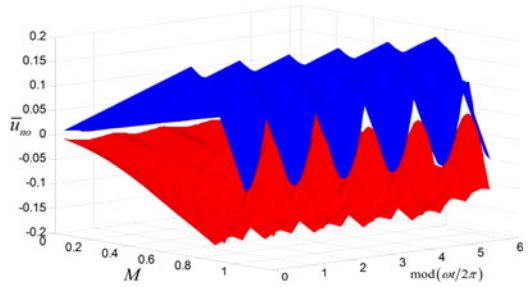

Fig. 7. Range of $u_{\rm no}$ based on RCMV-CBM2.

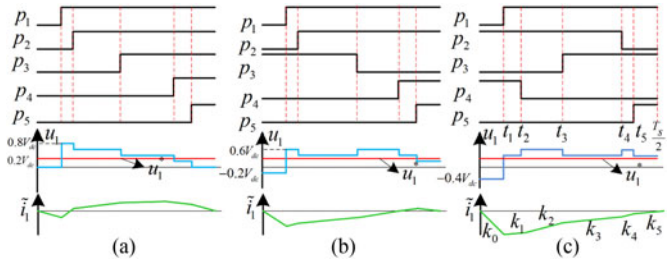

Fig. 8. Schematic diagram of output current ripple under three methods. (a) Generalized CBM. (b) RCMV-CBM1. (c) RCMV-CBM2.

Therefore, $u_{\rm no}$ for implementing RCMV-CBM2 is always available. The range of $\bar{u}_{\rm no}$ is depicted in Fig. 7. It is clear that the range of $\bar{u}_{\rm no}$ under RCMV-CBM2 is narrower than that of RCMV-CBM1. Meanwhile, RCMV-CBM1 has a greater optimization space than that of RCMV-CBM2 for performance improvement.

IV. Current Ripple Analysis

Different modulation strategies lead to different performance of power converter, such as the CMV characteristics, currents quality, power losses, and so on. The proposed RCMV-CBM1 and RCMV-CBM2 can reduce the CMV of the five-phase VSI effectively, but they will pose a negative effect on current quality. The purposes of this section are: 1) evaluating the current quality under the modulation methods presented in the previous sections; 2) optimizing the modulation strategies to improve the quality of output currents.

A. Calculation of Current Ripple

Usually, current total harmonic distortion (THD) is used to measure the quality of currents:

$$\mathrm{THD}_F = \frac{\sqrt{I_2^2 + I_3^2 + I_4^2 + \cdots}}{I_1}. \tag{18}$$

For the inverter with PWM, the average output currents over a switching period are equal to the reference currents. If the reference currents are sinusoidal, the current THD could be rewritten as [46]

$$\mathrm{THD}_F = \frac{\sqrt{\frac{1}{T}\int_0^T \left(i(t) - i^*(t)\right)^2 dt}}{I^*} \tag{19}$$

where $i(t)$ is the output current of the inverter in the steady state, $i^*(t)$ is the referenced sinusoidal current, and I^* represents the rms value of $i^*(t)$.

Refer to [39], the instantaneous current ripple $\tilde{i}(t)$ is defined as

$$\tilde{i}(t) = i(t) - i^*(t) \approx \frac{1}{L}\int_0^t \tilde{u}\,(\tau)d\tau \tag{20}$$

where $\tilde{u}(t) = u(t) - u^*(t)$, which is the error between the real and the referenced output voltages.

According to (19) and (20), to improve the quality of currents, the rms value of $\tilde{i}(t)$ over a modulation period must be minimized. If the switching sequence is symmetrical, the rms value of the current ripple over a half modulation period equals to that over a modulation period. Therefore, we only need to analyze the current ripple over a half-modulation period. Fig. 8 shows the output current ripple of a five-phase VSI under the three methods mentioned before.

The rms value of current ripple of phase-*j* over a modulation period [47]–[51] can be expressed as

$$\tilde{I}_j^2 = \frac{2}{T_s}\int_0^{\frac{T_s}{2}} \tilde{i}_j(t)^2 dt,\ j \in S = \{1, 2, \ldots, 5\}. \tag{21}$$

From the definition of current ripple in (20), we take RCMV-CBM2 as an example to illustrate the current ripple calculation of phase-p_1.

First, the voltage error in phase-p_1 needs to be calculated. According to Fig. 8, $\tilde{u}_1$ is a staircase function and it can be described as

$$\tilde{u}_1 = \begin{cases} -\frac{2}{5}V_{\rm dc} - u_1^*,\ t \in [0,\ t_1) \\ \frac{2}{5}V_{\rm dc} - u_1^*,\ t \in [t_1, t_2) \\ \frac{3}{5}V_{\rm dc} - u_1^*,\ t \in [t_2, t_3) \\ \frac{2}{5}V_{\rm dc} - u_1^*,\ t \in [t_3, t_4) \\ \frac{3}{5}V_{\rm dc} - u_1^*,\ t \in [t_4, t_5) \\ \frac{2}{5}V_{\rm dc} - u_1^*,\ t \in \left[t_5, \frac{T_s}{2}\right] \end{cases} \tag{22}$$

where $t_1 - t_5$ can be calculated from (13) and Fig. 6, and both are linear function of $u_{\rm no}$.

Hence, from (20)–(22), $\tilde{I}_1^2$ is deduced as

$$\tilde{I}_1^2 = \frac{2}{T_s}\left\{\begin{array}{l} \int_0^{t_1} (k_0 t)^2 dt + \int_{t_1}^{t_2} \left(k_1\,(t - t_1) + k_0 t_1\right)^2 dt + \\ \int_{t_2}^{t_3} \left(k_2\,(t - t_2) + k_1\,(t_2 - t_1) + k_0 t_1\right)^2 dt + \cdots \\ \int_{t_5}^{\frac{T_s}{2}} \left(k_5\,(t - t_5) + k_4\,(t_5 - t_4) + \cdots + k_1\,(t_2 - t_1)\right. \\ \left. + k_0 t_1\right)^2 dt \end{array}\right\} \tag{23}$$

where $k_0 - k_5$ are the slope of $\tilde{i}_1(t)$, and they are relying on the voltage error in (22), $k = \tilde{u}_1/L$.

By analogy, $\tilde{I}_j^2\,(j \in S)$ under the generalized CBM, RCMV-CBM1, and RCMV-CBM2 can be obtained in the same way.

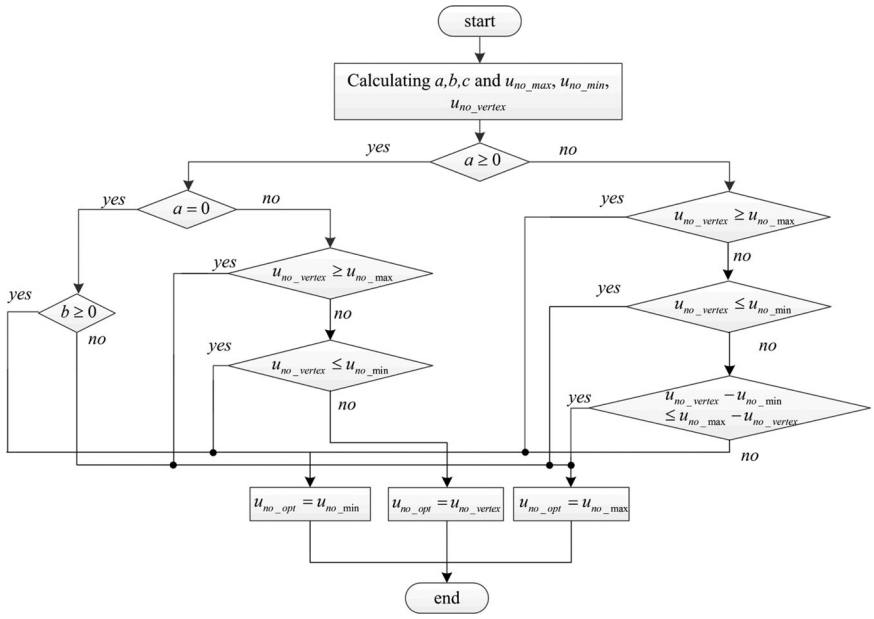

Fig. 9. Flowchart for calculating the optimal solution.

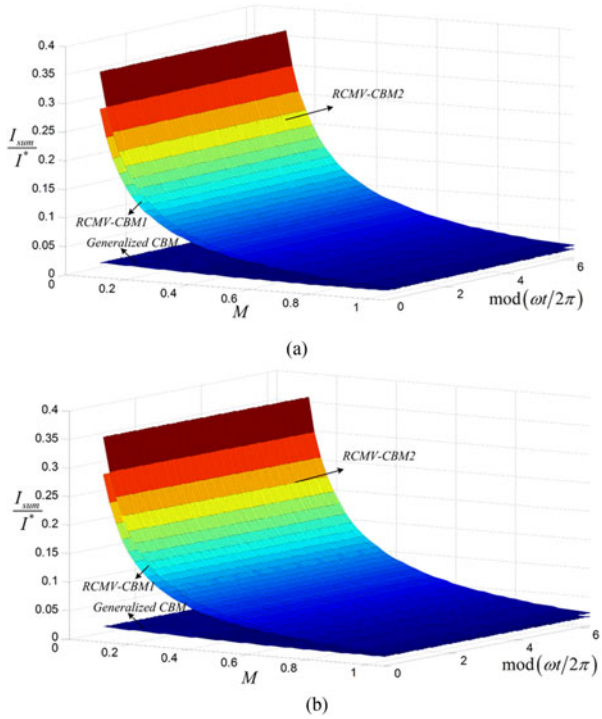

Fig. 10. Current ripple comparison of three methods. (a) Standard solution. (b) Optimal solution.

B. Minimum Current Ripple

There are five output phases in the studied system. Thus, to evaluate and optimize the three methods, the sum of five phases' rms value of current ripple is expressed as

$$I_{\rm sum} = \sqrt{\sum_{j \in S} \tilde{I}_j^2}. \tag{24}$$

Based on the above-mentioned analysis, it can be found that the rms value of current ripple is a quadratic function of $u_{\rm no}$. That is to say, the current ripple could be reduced by choosing a proper $u_{\rm no}$. Therefore, it can be transformed into a constrained optimal problem, and it is formulated as follows:

$$\begin{aligned} &\text{minimize } {I_{\rm sum}}^2 \\ &\text{subject to (6) or (14) or (17).} \end{aligned} \tag{25}$$

The three presented methods have different constraints for $u_{\rm no}$. As for the generalized CBM method, (6) should be met. As for RCMV-CBM1 and RCMV-CBM2, (14) and (17) should be satisfied, respectively.

Based on (23), the trajectories of the objective function are parabolas at any instants and M below 1.0515, so it can be written as

$$f\left(u_{\rm no}\right) = a{u_{\rm no}}^2 + bu_{\rm no} + c \tag{26}$$

where the coefficients "a," "b," and "c" can be calculated with (21)–(24), the vertex of the parabolas is $u_{\rm no\_vertex} = b/2a$. There are only some cumbersome calculations involved for obtaining of the coefficients, so the calculation results of three methods are listed in the Appendix.

The flowchart for obtaining the optimal solution $u_{\rm no\_opt}$ is shown in Fig. 9. As seen, the optimal solution will appear at three points: the upper boundary point $(u_{\rm no\_max})$, the lower boundary point $(u_{\rm no\_min})$, and the extreme point $(u_{\rm no\_vertex})$.

C. Current Quality Comparison of Three Methods

Based on the definition formula of THD in (20), the ratio $I_{\rm sum}/I*$ can be employed to measure the quality of output

TABLE II
SWITCHING STATE COMBINATIONS UNDER RCMV-CBM2

Sector	Voltages order	Switching state combinations ($S_{\mathrm{A}p}S_{\mathrm{B}p}S_{\mathrm{C}p}S_{\mathrm{D}p}S_{\mathrm{E}p}$)					
		Vector1	Vector2	Vector3	Vector4	Vector5	Vector6
1	[A,B,E,C,D]	(01100)	(11100)	(11000)	(11001)	(10001)	(10011)
2	[B,A,C,E,D]	(10001)	(11001)	(11000)	(11100)	(01100)	(01110)
3	[B,C,A,D,E]	(00110)	(01110)	(01100)	(11100)	(11000)	(11001)
4	[C,B,D,A,E]	(11000)	(11100)	(01100)	(01110)	(00110)	(00111)
5	[C,D,B,E,A]	(00011)	(00111)	(00110)	(01110)	(01100)	(11100)
6	[D,C,E,B,A]	(01100)	(01110)	(00110)	(00111)	(00011)	(10011)
7	[D,E,C,A,B]	(10001)	(10011)	(00011)	(00111)	(00110)	(01110)
8	[E,D,A,C,B]	(00110)	(00011)	(00011)	(10011)	(10001)	(11001)
9	[E,A,D,B,C]	(11000)	(11001)	(10001)	(10011)	(00011)	(00110)
10	[A.E,B,D,C]	(00011)	(10011)	(10001)	(11001)	(11000)	(11100)

Note: voltages order [A,B,E,C,D] denotes that the output voltages are sorted from large to small, namely $u^*_{\mathrm{AN}} \geq u^*_{\mathrm{BN}} \geq u^*_{\mathrm{EN}} \geq u^*_{\mathrm{CN}} \geq u^*_{\mathrm{DN}}$.

TABLE III
PARAMETERS USED IN THE EXPERIMENTS

Parameters	Value
DC voltage	100 V
Load inductance (L_o)	3.6 mH
Load resistor (R_o)	6 Ω
Sampling frequency (f_s)	10 kHz

currents. $I*$ is expressed as

$$I^* = \frac{MV_{\mathrm{dc}}}{\sqrt{2}\,|Z_L|} \tag{27}$$

where Z_L is the load impedance, when the balanced five-phase *RL* load is adopted, $|Z_L| = \sqrt{R^2 + (\omega_o L)^2}$.

It is clear that once the switching state sequence is determined, $\tilde{I}_j^2$ can be determined by the selection of zero-sequence signal u_{no}. To compare the current quality of the three methods, u_{no} should be determined first. Actually, two kinds of solutions can be used for comparison, namely, the optimal solution and the unified solution. The optimal solution can be obtained by Section IV-B. As for the latter one, all the feasible solution in Fig. 7 can be used, because the feasible solution of RCMV-CBM2 is the subset of that under generalized CBM and RCMV-CBM1. In particular, u_{no} is selected at $\lambda = 0.5$ (named as the standard solution).

The three-dimensional diagram of I_{sum}/I^* with respect to *M* and ωt under two different solutions is illustrated in Fig. 10. As seen, there is no significant difference between Fig. 10(a) and (b). By subtraction, we can find that the ratio I_{sum}/I^* under optimal solution is slightly less than that of standard solution. Under both the standard and optimal solutions, it can be found that at any instants and M, I_{sum}/I^* of generalized CBM is smaller than that of RCMV-CBM1 that is then smaller than that of RCMV-CBM2. In addition, it is worth noting that I_{sum}/I^* under three methods become closer as *M* increases. As a conclusion, the generalized CBM is superior to RCMV-CBM1 and RCMV-CBM2 in current quality, and the current quality of three methods is better as *M* increases.

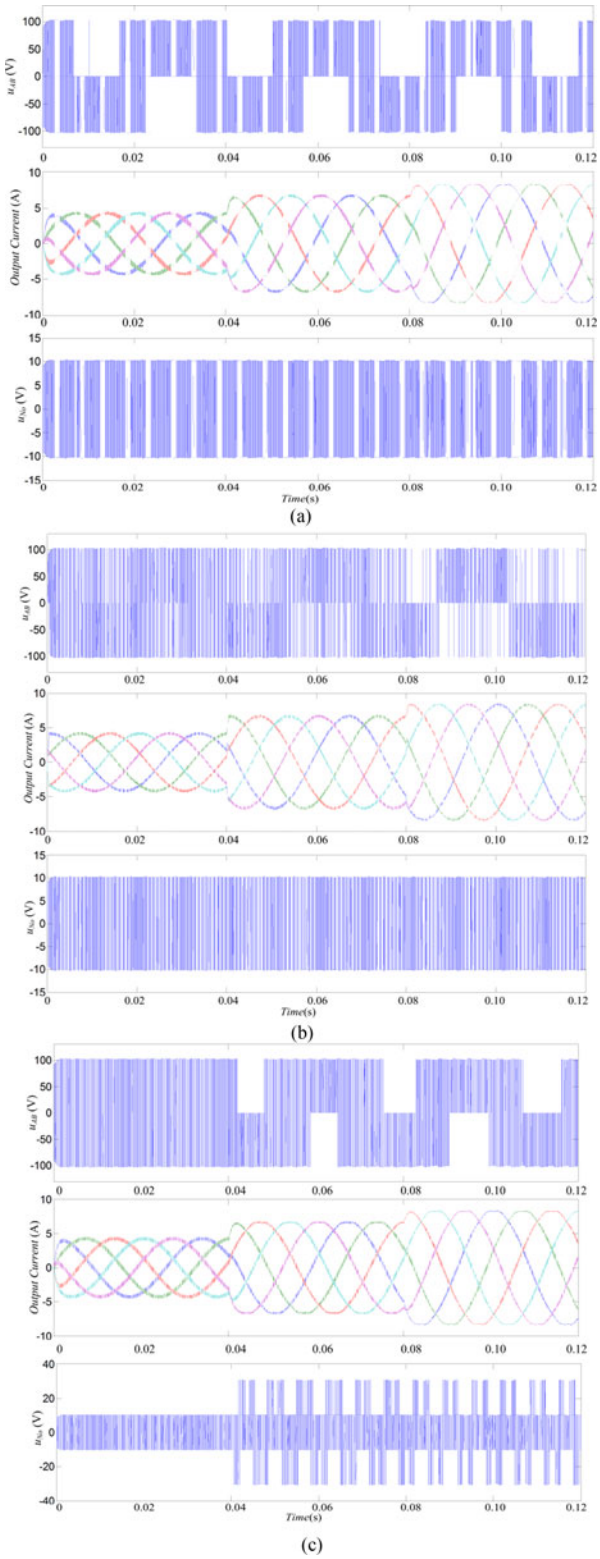

Fig. 11. Simulation results. (a) RCMV-CBM2. (b) MPC. (c) PS-CBM.

V. COMPARISONS WITH OTHER REDUCED CMV METHODS

In this section, the comparisons are performed among the four methods: the RCMV-CBM2 method, MPC method [40], PS-CBM method [41], and SVM method [42].

TABLE IV
OUTPUT CURRENT THD ANALYSIS OF DIFFERENT CMV REDUCED METHODS

Condition	Method	THD of i_A	THD of i_B	THD of i_C	THD of i_D	THD of i_E
$M = 0.5$, $f_o = 30$ Hz	RCMV-CBM2	3.05%	3.05%	3.04%	3.05%	3.04%
	MPC [40]	2.47%	2.45%	2.5%	2.45%	2.48%
	PS-CBM [41]	3.04%	3.06%	3.04%	3.04%	3.05%
$M = 0.8$, $f_o = 30$ Hz	RCMV-CBM2	1.63%	1.63%	1.62%	1.62%	1.63%
	MPC [40]	1.62%	1.62%	1.63%	1.63%	1.65%
	PS-CBM [41]	1.74%	1.80%	1.74%	1.74%	1.81%
$M = 1.0$, $f_o = 30$ Hz	RCMV-CBM2	1.34%	1.34%	1.35%	1.35%	1.34%
	MPC [40]	1.27%	1.21%	1.26%	1.25%	1.21%
	PS-CBM [41]	1.32%	1.40%	1.32%	1.33%	1.40%

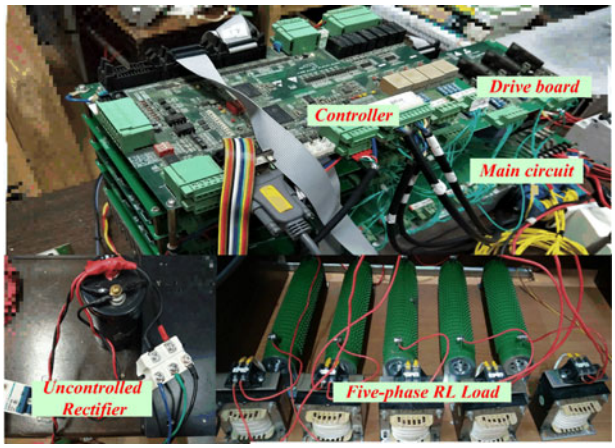

Fig. 12. Experimental setup for the five-phase VSI.

A. Theoretical Analysis

In the SVM method with minimum CMV in [42], six adjacent large space vectors are utilized. Two of them are in opposite phase and have the same duty ratios. It is not difficult to find that six different switching state combinations are also utilized per carrier period under RCMV-CBM2. From Fig. 6, the specific switching state combinations under different desired voltage sector are listed in Table II. After comparisons, it is obtained that the adopted switching state combinations in RCMV-CBM2 are the same as those in the SVM method in [42]. Furthermore, when the zero sequence signal is selected as the standard solution, RCMV-CBM2 is equivalent to the SVM method [42]. Thus, it can be concluded that RCMV-CBM2 will be superior to the SVM method in [42] in current quality, when the optimal solution is used for RCMV-CBM2.

As for the MPC method in [40], the cost function is constructed by two parts: the current error in two transformation planes and different weights of switching state combinations in different groups (group 1, group 2, group 3). The minimum CMV can be achieved through selecting a proper weight of the second part. The solution set consists of 32 switching state combinations, which will cause a large computational burden for the controller. In addition, there may be more than one switch conducted or no switch conducted during two control periods. Thus, the switching frequency under MPC method is not fixed. In fact, by restricting the solution set in group 3, the minimum peak-to-peak value of CMV can be obtained, and the computational burden of the controller will be mitigated to some extent.

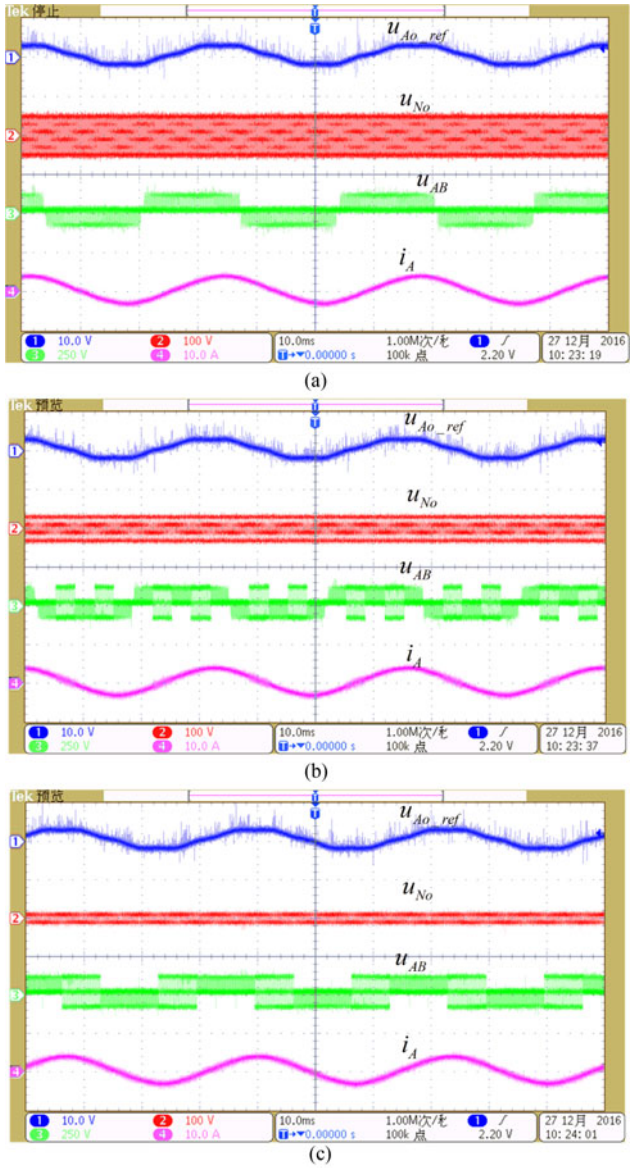

Fig. 13. Related waveforms under case I with standard solution. (a) Generalized CBM. (b) RCMV-CBM1. (c) RCMV-CBM2.

In the PS-CBM method [41], five different carriers are utilized, and the phase shift of each carrier is one-fifth of the carrier period. Because the sinusoidal desired voltages are adopted, $M_{\max}$ is limited to unity. As M increases, the number of overlapping areas increases. Therefore, the peak-to-peak value of CMV will change from 0.2 to 0.6 $V_{\rm dc}$. Namely, the PS-CBM method cannot achieve the minimum CMV in the whole range of M.

B. Simulation Comparisons

To compare the current quality of RCMV-CBM2, the MPC method [40], and the PS-CBM method in [41], simulations are carried out based on MATLAB/Simulink. The related parameters are listed in Table III. To ensure that six switching state combinations are adopted in each carrier period, the

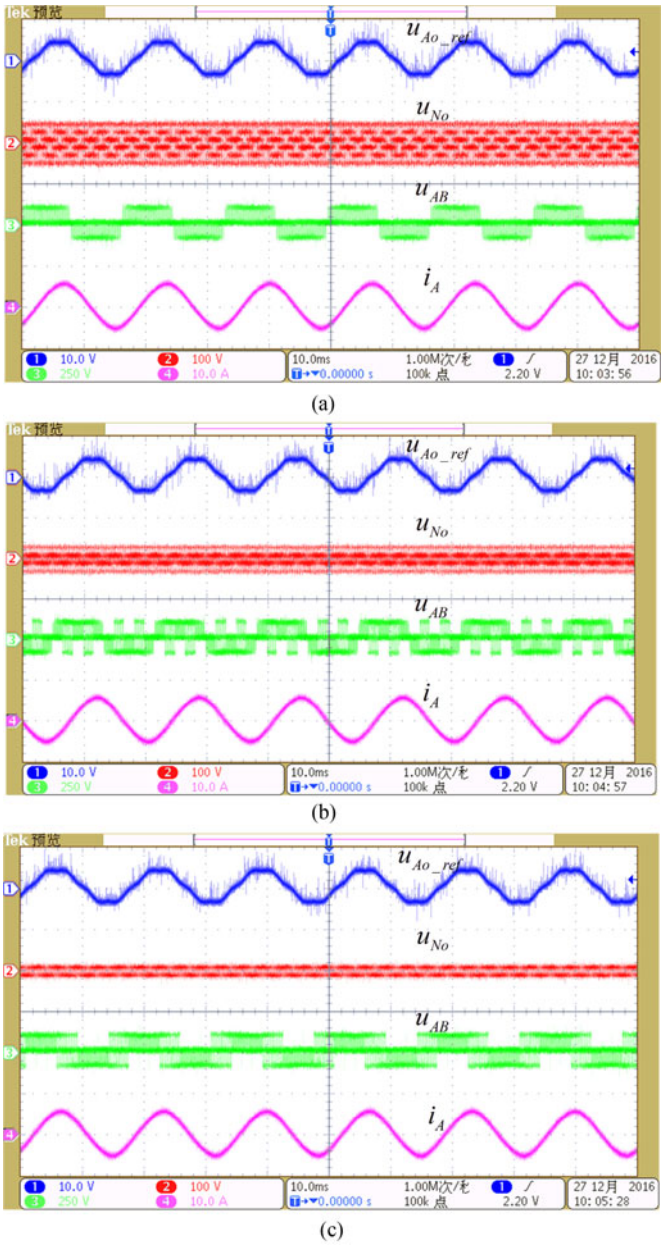

Fig. 14. Related waveforms under case II with standard solution. (a) Generalized CBM. (b) RCMV-CBM1. (c) RCMV-CBM2.

control period (T_c) of the MPC method is set to one-sixth of the carrier period (T_s) of RCMV-CBM2 and PS-CBM. The optimal solution is used to implement RCMV-CBM2.

The simulation results are illustrated in Fig. 11. The output frequency is set to 30 Hz, and *M* is set to 0.5 during 0–0.04 s, 0.8 during 0.04–0.08 s, and then changed to 1.0 at 0.08 s. As seen, all the methods can obtain sinusoidal output currents, but the output line-to-line voltages are totally different. The RCMV-CBM2 method and MPC method can obtain the minimum CMV in the whole range of *M*, but the PS-CBM method cannot. The THDs of the output currents under the above-mentioned methods are listed in Table IV, which demonstrate that the current quality under RCMV-CBM2 and the PS-CBM method is roughly the same. The MPC method has the best current quality owing to that

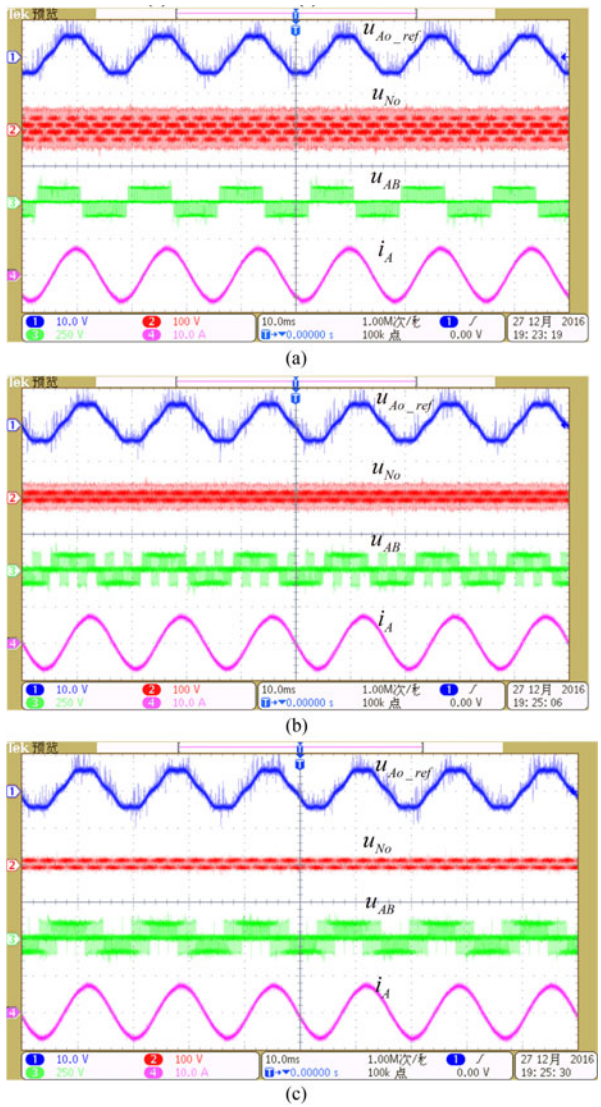

Fig. 15. Related waveforms under case III with standard solution. (a) Generalized CBM. (b) RCMV-CBM1. (c) RCMV-CBM2.

$T_c = 1/6T_s$ is adopted in this simulation. It is worth noting that the current quality advantage of the MPC method is gradually fading with the increase of *M*. Moreover, if the control period of the MPC method is set as $T_c = T_s$, the current quality will become even worse.

In summary, RCMV-CBM2 has an excellent comprehensive performance, because it could achieve: 1) the minimum CMV in whole range of *M*; 2) uniform power losses distribution in each phase; and 3) relatively low current THD.

VI. Experiment Results

A. Experimental Setup

To validate the proposed methods, an experimental setup for the five-phase VSI is developed in the laboratory, as shown in Fig. 12. The setup includes: controller board, main circuit board, drive boards, uncontrolled rectifier, and a five-phase balanced *RL* load. The controller board is mainly composed of a

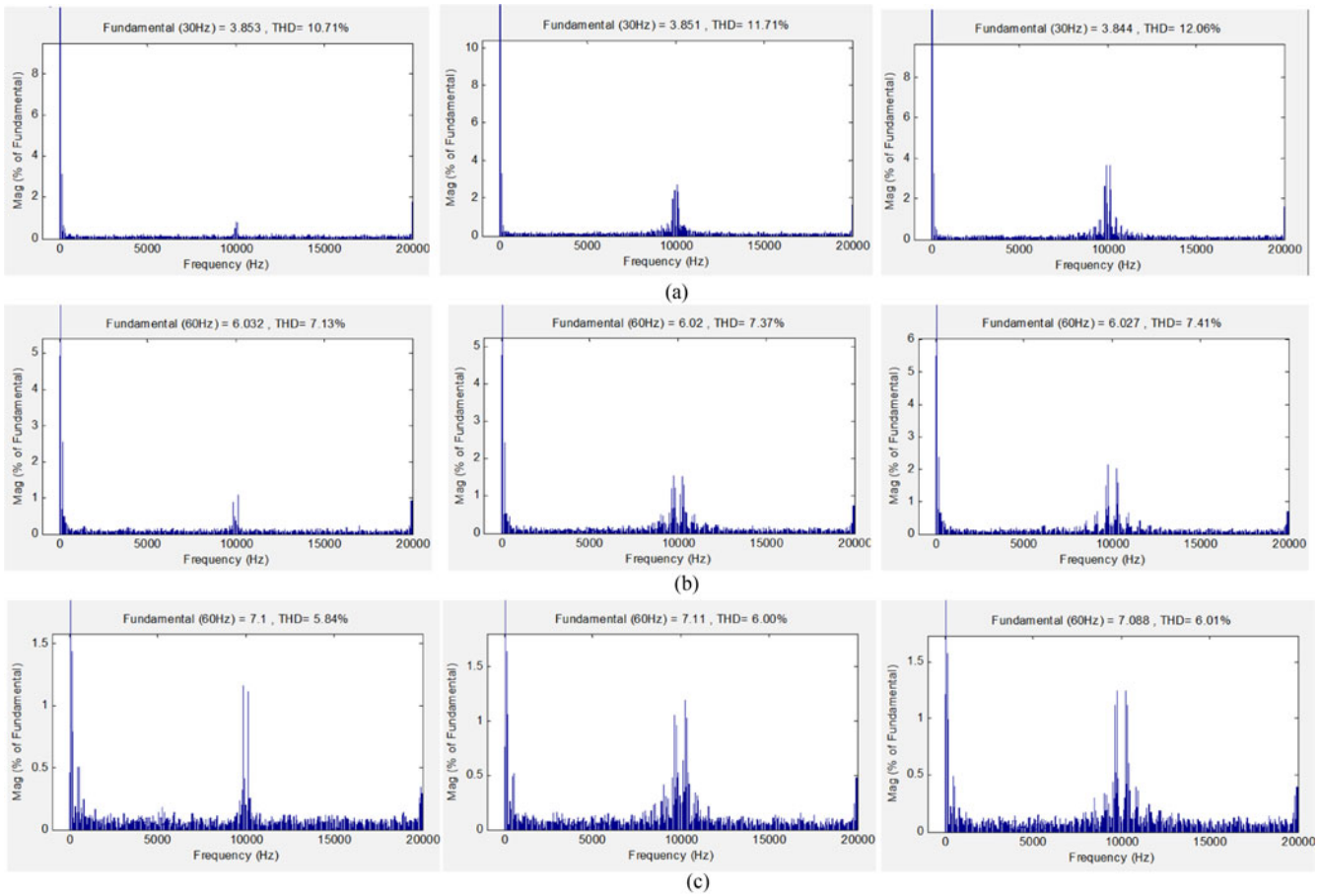

Fig. 16. Spectrum graphics of the input currents i_A under generalized CBM (left), RCMV-CBM1 (middle), RCMV-CBM2 (right). (a) Case I, (b) case II, and (c) case III.

floating-point DSP (TMS320F28335) and a field programmable gate array (FPGA) (EP2C8J144C8N). The DSP is responsible for the related calculation, and FPGA is used to generate PWM signals. The unidirectional power switches in the five-phase VSI are implemented by the insulated gate bipolar transistor IHW30N120R2 (1200 V/30 A, Infineon). The related parameters are listed in Table III. The carrier frequency is equal to the sampling frequency.

To avoid the shoot-through of a VSI, a dead time T_d should be inserted in each leg. As a result, the CMV characteristic will be away from the expectation, and the output currents will be distorted. There are many dead-time compensation methods to address this issue. In this paper, the dead-time is eliminated by the detection of output current polarity [52].

Two different selections of zero-sequence signal are adopted in experiments: the standard solution and the optimal solution.

B. Experimental Results With the Standard Solution

The experiments are carried out in the following cases:

1) $M = 0.5$, $f_o = 30$ Hz;
2) $M = 0.8$, $f_o = 60$ Hz;
3) $M = 1.0515$, $f_o = 60$ Hz; and
4) Different M under $f_o = 60$ and 30 Hz.

The measured waveforms with three CBM methods under case I are shown in Fig. 13. From top to bottom, they are modulated voltage $u_{\mathrm{Ao\_ref}}$, the CMV u_{No}, output line-to-line voltage u_{AB}, and output current i_A. The modulated signals of three methods are the same. As seen, the sinusoidal output currents are achieved under three methods. The waveforms of u_{AB} and u_{No} are totally different under three methods. The peak-to-peak value of CMV is nearly 122 V under the generalized CBM, 78 V in RCMV-CBM1, and 28 V in RCMV-CBM2, which are in accordance with the theoretical analysis.

When the modulation index is changed to 0.8 and the output frequency equal to 60 Hz, the measured waveforms with different modulation strategies are shown in Fig. 14. With the increase of modulation index, the waveforms of output current become smoother than those in case I. The CMV characteristics are similar with case I, which also prove the effectiveness of proposed methods. In addition, the measured waveforms under case III are shown in Fig. 15, which can verify the effectiveness of proposed methods under the maximum modulation index.

The differences of the current ripples under different methods can be obtained from the spectral analysis. By importing the data of output currents into MATLAB, the spectral analysis results of output current i_A with three methods under case I,

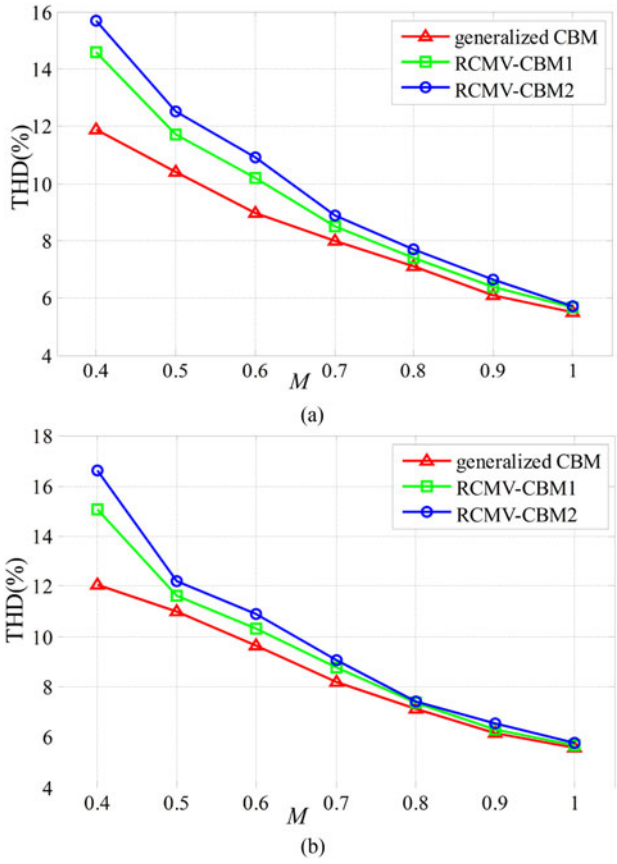

Fig. 17. Measured THD of output currents. (a) $f_o = 30$ Hz. (b) $f_o = 60$ Hz.

case II, and case III are shown in Fig. 16. It can be learned that the low-frequency harmonic components of three methods are basically identical. However, the harmonic components around the switching frequency are significantly different. RCMV-CBM2 has the highest amplitude of the harmonic components around the switching frequency, and the generalized CBM has the lowest.

To evaluate the harmonic performance of three methods more intuitively, the THDs of the output currents under different *M* and frequencies (case IV) are shown in Fig. 17. As seen, the generalized CBM is superior to RCMV-CBM1 and RCMV-CBM2 in current quality, which is in accordance with the theoretical analysis in Section IV. In addition, it can be found that the output current quality becomes better with the increase of modulation index *M*.

C. Experimental Results With the Optimal Solution

In this experiment, the optimal $u_{\rm no}$ for three CBM methods are adopted. The waveforms of the three CBM methods under case II are illustrated in Fig. 18. The sinusoidal output currents are achieved under the three methods, the peak-to-peak values of CMV of the three methods are in accordance with the standard solution. The modulated signals of three CBM methods are totally different. Under the generalized CBM, its optimal solution is $u_{\rm no} = 0$ when *M* is less than unity [40]. Hence, we can find the modulated signals of the generalized

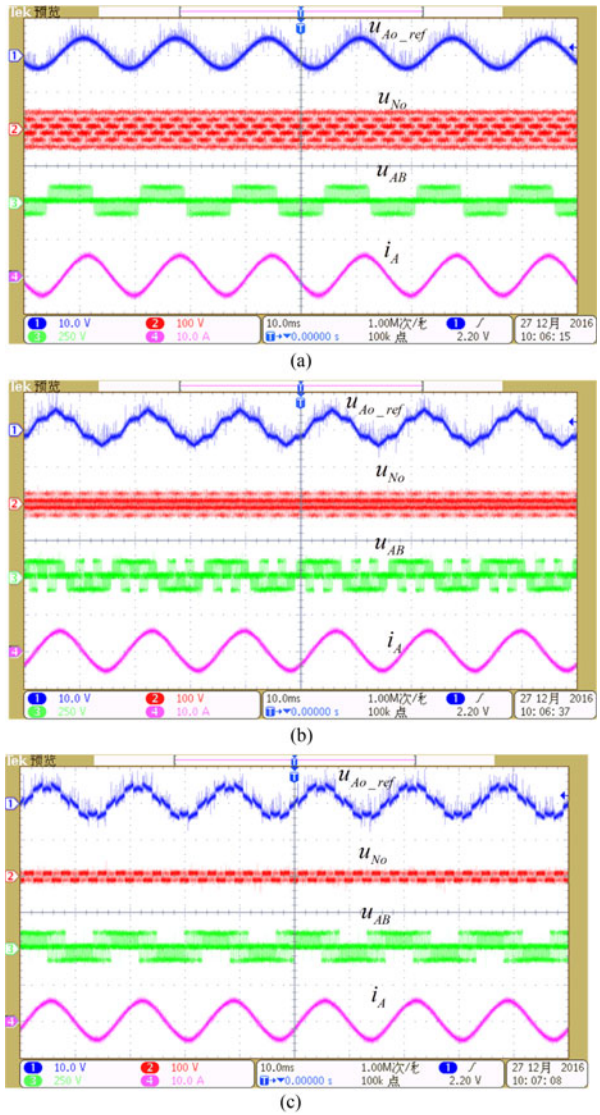

Fig. 18. Related waveforms under case II with optimal solution. (a) Generalized CBM. (b) RCMV-CBM1. (c) RCMV-CBM2.

TABLE V
OUTPUT CURRENT THD ANALYSIS WITH DIFFERENT ZERO SEQUENCE SIGNALS

Method	Selection of $u_{\rm no}$	THD of i_A Case I	Case II	Case III
Generalized CBM	Standard Solution	10.71%	7.13%	5.84%
	Optimal Solution	10.12%	6.72%	5.80%
RCMV-CBM1	Standard Solution	11.71%	7.37%	6.0%
	Optimal Solution	11.38%	6.93%	5.93%
RCMV-CBM2	Standard Solution	12.06%	7.41%	6.01%
	Optimal Solution	11.63%	7.05%	5.97%

CBM shown in Fig. 18(a) are sinusoidal. The modulated signals of RCMV-CBM1 and RCMV-CBM2 are totally different from the modulated signals under standard solution. Different modulated signals correspond to different modulation strategies with different performance. The THD of the output currents under standard solution and optimal solution is listed in Table V. As

seen, the current quality of optimal solution is slightly better than that of standard solution, which is in accordance with the theoretical analysis in Section IV-C.

VII. Conclusion

In this paper, three modulation strategies based on CBM scheme are presented for a five-phase VSI: generalized CBM, RCMV-CBM1, and RCMV-CBM2, which are easier to implement than the corresponding SVM methods. The RCMV-CBM1 and RCMV-CBM2 methods are tailored for a five-phase VSI to reduce the CMV. By using the opposite carrier in one output phase, RCMV-CBM1 reduces the peak-to-peak value of CMV by 40%. In RCMV-CBM2, the opposite carrier is applied to two output phases, then the peak-to-peak value of CMV is further reduced by 80%. All the three methods can reach the maximum modulation index of 1.0515, RCMV-CBM1 and RCMV-CBM2 could reduce the CMV in the whole modulation range. Compared to the MPC method in [40], RCMV-CBM2 reduces the computation burden greatly and has uniform loss distribution. The selection of zero-sequence signal is a degree of freedom for the performance optimization, such as current quality and efficiency. Under the designed switching sequence, the optimal solution to improve the current quality can be obtained by minimizing the current ripple. Based on the current ripple analysis, it can be concluded that under the standard or the optimal zero-sequence signal, the generalized CBM method has better current quality than RCMV-CBM1; while RCMV-CBM1 has better current quality than RCMV-CBM2.

Furthermore, the concept of RCMV-CBM1 and RCMV-CBM2 presented for the five-phase VSI can also be extended to the other multiphase VSI, especially with odd phase number. Moreover, based on the equivalency of CBM and SVM, it is easy to derive the SVM methods which are equivalent to RCMV-CBM1 and RCMV-CBM2.

Appendix

The coefficients "*a*," "*b*," and "*c*" can be calculated by combining (21)–(24), then the coefficients under three methods are listed as follows.

For generalized CBM

$$a=\frac{5T_s^2M^2}{32L^2};\ b=0;$$
$$c=\frac{T_s^2{V_{\rm dc}}^2}{L^2}\begin{bmatrix}\frac{5}{512}M^4-\frac{391}{18181}M^3\cos\left(\theta-(2k\ -\ 1)\frac{\pi}{10}\right)+\\ \frac{34}{12417}M^3\cos\left(3\theta-(2k\ -\ 1)\frac{3\pi}{10}\right)+\frac{5}{384}M^2\end{bmatrix}. \quad \text{(A.1)}$$

For RCMV-CBM1

$$a=\frac{T_s^2}{L^2}\left(\frac{5}{32}M^2+\frac{311}{2021}M\cos\left(\theta-(2k\ -\ 1)\frac{\pi}{10}\right)-\frac{1}{5}\right)$$
$$b=\frac{T_s^2V_{\rm dc}}{L^2}\begin{pmatrix}\frac{-307}{9048}M^2\cos\left(2\theta-(4k\ +\ 3)\frac{\pi}{10}\right)\\ +\frac{3}{40}M\cos\left(\theta-(k\ +\ 2)\frac{\pi}{5}\right)\end{pmatrix}\cdot{\rm sign}_k$$
$$c=\frac{T_s^2{V_{\rm dc}}^2}{L^2}\begin{bmatrix}\frac{5}{512}M^4-\frac{94}{7097}M^3\cos\left(\theta-(2k\ -\ 1)\frac{\pi}{10}\right)\\ -\frac{16}{6533}M^3\cos\left(3\theta-(2k\ -\ 1)\frac{3\pi}{10}\right)\\ +\frac{3}{320}M^2\cos\left(2\theta-(2k\ -\ 1)\frac{\pi}{5}\right)-\frac{23}{1920}M^2+\frac{1}{60}\end{bmatrix}. \quad \text{(A.2)}$$

For RCMV-CBM2

$$a=\frac{T_s^2}{L^2}\left(\frac{5}{32}M^2+\frac{493}{1980}M\cos\left(\theta-(2k\ -\ 1)\frac{\pi}{10}\right)-\frac{3}{10}\right)$$
$$b=\frac{T_s^2V_{\rm dc}}{L^2}\begin{pmatrix}\frac{211}{10062}M^2\cos\left(2\theta-(4k\ +\ 3)\frac{\pi}{10}\right)\\ -\frac{323}{7985}M\cos\left(\theta-(k\ +\ 2)\frac{\pi}{5}\right)\end{pmatrix}\cdot{\rm sign}_k$$
$$c=\frac{T_s^2{V_{\rm dc}}^2}{L^2}\begin{bmatrix}\frac{5}{512}M^4-\frac{12}{6533}M^3\cos\left(\theta-(2k\ -\ 1)\frac{\pi}{10}\right)\\ -\frac{10}{14253}M^3\cos\left(3\theta-(2k\ -\ 1)\frac{3\pi}{10}\right)\\ +\frac{48}{24853}M^2\cos\left(2\theta-(2k\ -\ 1)\frac{\pi}{5}\right)-\frac{47}{1920}M^2+\frac{1}{40}\end{bmatrix} \quad \text{(A.3)}$$

where $\theta=\omega t$, $k\,(k\ =\ 1,\ 2,\ldots,\ 10)$ is the sector number of the desired output voltages, which can refer to Fig. 2, and ${\rm sign}_k=\begin{cases}1, k=1,3,5,7,9\\ -1, k=2,4,6,8,10\end{cases}$.

References

[1] U. T. Shami and H. Akagi, "Experimental discussions on a shaft end-to-end voltage appearing in an inverter-driven motor," *IEEE Trans. Power Electron.*, vol. 24, no. 6, pp. 1532–1540, Jun. 2009.

[2] F. J. T. E. Ferreira, M. V. Cistelecan, and A. T. De Almeida, "Evaluation of slot-embedded partial electrostatic shield for high-frequency bearing current mitigation in inverter-fed induction motors," *IEEE Trans. Energy Convers.*, vol. 27, no. 2, pp. 382–390, Jun. 2012.

[3] H. Akagi and T. Shimizu, "Attenuation of conducted EMI emissions from an inverter-driven motor," *IEEE Trans. Power Electron.*, vol. 23, no. 1, pp. 282–290, Jan. 2008.

[4] H. Zhang and A. von Jouanne, "Suppressing common-mode conducted EMI generated by PWM drive systems using a dual-bridge inverter," in *Proc. 13th Annu. Appl. Power Electron. Conf. Expo.*, 1998, pp. 1017–1020.

[5] S. Ogasawara, H. Ayano, and H. Akagi, "An active circuit for cancellation of common-mode voltage generated by a PWM inverter," in *Proc. Rec. 28th Annu. IEEE Power Electron. Spec. Conf.*, 1997, pp. 1547–1553.

[6] A. L. Julian, G. Oriti, and T. A. Lipo, "Elimination of common mode voltage in three phase sinusoidal power converters," *IEEE Trans. Power Electron.*, vol. 14, no. 5, pp. 982–989, Sep. 1999.

[7] C. T. Morris, D. Han, and B. Sarlioglu, "Reduction of common mode voltage and conducted EMI through three phase inverter topology," *IEEE Trans. Power Electron.*, vol. 32, no. 3, pp. 1720–1724, Mar. 2017.

[8] C. Tan, D. Xiao, J. E. Fletcher, and M. F. Rahman, "Analytical and experimental comparison of carrier-based PWM methods for the five-phase coupled-inductor inverter," *IEEE Trans. Ind. Electron.*, vol. 63, no. 12, pp. 7328–7338, Dec. 2016.

[9] J. Huang and H. Shi, "A hybrid filter for the suppression of common-mode voltage and differential-mode harmonics in three-phase inverters with CPPM," *IEEE Trans. Ind. Electron.*, vol. 62, no. 7, pp. 3991–4000, Jul. 2015.

[10] G. Ala, G. C. Giaconia, G. Giglia, M. C. Di Piazza, and G. Vitale, "Design and performance evaluation of a high power-density EMI filter for PWM inverter-fed induction-motor drives," *IEEE Trans. Ind. Appl.*, vol. 52, no. 3, pp. 2397–2404, May/Jun. 2016.

[11] A. M. Hava and E. Un, "Performance analysis of reduced common-mode voltage PWM methods and comparison with standard PWM methods for three-phase voltage-source inverters," *IEEE Trans. Power Electron.*, vol. 24, no. 1, pp. 241–252, Jan. 2009.

[12] E. Un and A. M. Hava, "A near-state PWM method with reduced switching losses and reduced common-mode voltage for three-phase voltage source inverters," *IEEE Trans. Ind. Appl.*, vol. 45, no. 2, pp. 782–793, Mar./Apr. 2009.

[13] A. M. Hava and E. Ün, "A high-performance PWM algorithm for common-mode voltage reduction in three-phase voltage source inverters," *IEEE Trans. Power Electron.*, vol. 26, no. 7, pp. 1998–2008, Jul. 2011.

[14] H. Chen and H. Zhao, "Review on pulse-width modulation strategies for common-mode voltage reduction in three-phase voltage-source inverters," *IET Power Electron.*, vol. 9, no. 14, pp. 2611–2620, 2016.

[15] Y. S. Lai, "New random technique of inverter control for common mode voltage reduction of inverter-fed induction motor drives," *IEEE Trans. Energy Convers.*, vol. 14, no. 4, pp. 1139–1146, Dec. 1999.

[16] H. Zhang, A. Von Jouanne, S. Dai, A. K. Wallace, and F. Wang, "Multilevel inverter modulation schemes to eliminate common-mode voltages," *IEEE Trans. Ind. Appl.*, vol. 36, no. 6, pp. 1645–1653, Nov. 2000.

[17] N. V. Nguyen, T. T. Nguyen, and H. H. Lee, "A reduced switching loss PWM strategy to eliminate common-mode voltage in multilevel inverters," *IEEE Trans. Power Electron.*, vol. 30, no. 10, pp. 5425–5438, Oct. 2015.

[18] R. M. Tallam, R. J. Kerkman, D. Leggate, and R. A. Lukaszewski, "Common-mode voltage reduction PWM algorithm for ac drives," *IEEE Trans. Ind. Appl.*, vol. 46, no. 5, pp. 1959–1969, Sep./Oct. 2010.

[19] C.-C. Hou, C.-C. Shih, P.-T. Cheng, and A. M. Hava, "Common-mode voltage reduction pulsewidth modulation techniques for three-phase grid-connected converter," *IEEE Trans. Power Electron.*, vol. 28, no. 4, pp. 1971–1979, Apr. 2013.

[20] G. Tan, X. Wu, Z. Wang, and Z. Ye. "A generalized algorithm to eliminate spikes of common-mode voltages for CMVRPWM," *IEEE Trans. Power Electron.*, vol. 31, no. 9, pp. 6698–6709, Sep. 2016.

[21] X. Wu, G. Tan, Z. Ye, Y. Liu, and S. Xu, "Optimized common-mode voltage reduction PWM for three-phase voltage-source inverters," *IEEE Trans. Power Electron.*, vol. 31, no. 4, pp. 2959–2969, Apr. 2016.

[22] J. W. Kimball and M. Zawodniok, "Reducing common-mode voltage in three-phase sine-triangle PWM with interleaved carriers," in *Proc. IEEE Appl. Power Electron. Conf. Expo.*, Palm Springs, CA, 2010, pp. 1508–1513.

[23] J. W. Kimball and M. Zawodniok, "Reducing common-mode voltage in three-phase sine-triangle PWM with interleaved carriers," *IEEE Trans. Power Electron.*, vol. 26, no. 8, pp. 1998–2008, Aug. 2011.

[24] J. Huang and H. Shi, "Suppressing low-frequency components of common mode voltage through reverse injection in three-phase inverter," *IET Power Electron.*, vol. 7, no. 6, pp. 1644–1653, Jun. 2014.

[25] J. Huang and H. Shi, "Reducing the common-mode voltage through carrier peak position modulation in an SPWM three-phase inverter," *IEEE Trans. Power Electron.*, vol. 29, no. 9, pp. 4490–4495, Sep. 2014.

[26] J. Huang and H. Shi, "Carrier multi-modulation used for the common mode voltage suppression in a three-phase inverter," in *Proc. IEEE Energy Convers. Congr. Expo.*, Montreal, QC, 2015, pp. 2084–2090.

[27] P. C. Loh, D. G. Homles, and T. A. Lipo, "Implementation and control of distributed PWM cascaded multilevel inverters with minimal harmonic distortion and common-mode voltage," *IEEE Trans. Power Electron.*, vol. 20, no. 1, pp. 90–99, Jan. 2005.

[28] S. R. Bowes and Y. S. Lai, "The relationship between space-vector modulation and regular-sampled PWM," *IEEE Trans. Power Electron.*, vol. 14, no. 5, pp. 670–679, Sep. 1997.

[29] K. Zhou and D. Wang, "Relationship between space-vector modulation and three-phase carrier-based PWM: A comprehensive analysis," *IEEE Trans. Ind. Electron.*, vol. 49, no. 1, pp. 186–196, Feb. 2002.

[30] E. Levi, "Multiphase electric machines for variable-speed applications," *IEEE Trans. Ind. Electron.*, vol. 55, no. 5, pp. 1893–1909, May 2008.

[31] A. Tani, M. Mengoni, L. Zarri, G. Serra, and D. Casadei, "Control of multiphase induction motors with an odd number of phases under open circuit phase faults," *IEEE Trans. Power Electron.*, vol. 27, no. 2, pp. 565–577, Feb. 2012.

[32] E. Levi, "Advances in converter control and innovative exploitation of additional degrees of freedom for multiphase machines," *IEEE Trans. Ind. Electron.*, vol. 63, no. 1, pp. 433–448, Jan. 2016.

[33] M. Mengoni, L. Zarri, A. Tani, L. Parsa, G. Serra, and D. Casadei, "High-torque-density control of multiphase induction motor drives operating over a wide speed range," *IEEE Trans. Ind. Electron.*, vol. 62, no. 2, pp. 814–825, Feb. 2015.

[34] S. Karugaba and O. Ojo, "A carrier-based PWM modulation technique for balanced and unbalanced reference voltages in multiphase voltage-source inverters," *IEEE Trans. Ind. Appl.*, vol. 48, no. 6, pp. 2102–2109, Nov./Dec. 2012.

[35] G. Renukadevi and K. Rajambal, "Field programmable gate array implementation of space-vector pulse-width modulation technique for five-phase voltage source inverter," *IET Power Electron.*, vol. 7, no. 2, pp. 376–389, Feb. 2014.

[36] A. Iqbal and S. Moinuddin, "Comprehensive relationship between carrier-based PWM and space vector PWM in a five-phase VSI," *IEEE Trans. Power Electron.*, vol. 24, no. 10, pp. 2379–2390, Oct. 2009.

[37] H. M. Ryu, J. H. Kim, and S. K. Sul, "Analysis of multiphase space vector pulse-width modulation based on multiple d–q spaces concept," *IEEE Trans. Power Electron.*, vol. 20, no. 6, pp. 1364–1371, Nov. 2005.

[38] K. Y. Chen and J. S. Hu, "A filtered SVPWM for multiphase voltage source inverters considering finite pulse-width resolution," *IEEE Trans. Power Electron.*, vol. 27, no. 7, pp. 3107–3118, Jul. 2012.

[39] K. Y. Chen, "Space-vector pulse-width modulation for multiphase voltage source inverters considering reference order," *IET Power Electron.*, vol. 9, no. 1, pp. 81–94, 2016.

[40] M. J. Duran, J. A. Riveros, F. Barrero, H. Guzman, and J. Prieto, "Reduction of common-mode voltage in five-phase induction motor drives using predictive control techniques," *IEEE Trans. Ind. Appl.*, vol. 48, no. 6, pp. 2059–2067, Nov./Dec. 2012.

[41] Z. Liu, Z. Zheng, S. D. Sudhoff, C. Gu, and Y. Li, "Reduction of common mode voltage in multiphase two-level inverters using SPWM with phase-shifted carriers," *IEEE Trans. Power Electron.*, vol. 31, no. 9, pp. 6631–6645, Sep. 2016.

[42] M. J. Duran, J. Prieto, F. Barrero, J. A. Riveros, and H. Guzman, "Space-vector PWM with reduced common-mode voltage for five phase induction motor drives," *IEEE Trans. Ind. Electron.*, vol. 60, no. 10, pp. 4159–4168, Oct. 2013.

[43] H. A. Hussain and H. A. Toliyat, "Reduction of shaft voltages and bearing currents in five-phase induction motors," in *Proc. IEEE Energy Convers. Congr. Expo.*, Raleigh, NC, Sep. 2012, pp. 3309–3316.

[44] N. Bodo, M. Jones, and E. Levi, "A space vector PWM with common-mode voltage elimination for open-end winding five-phase drives with a single dc supply," *IEEE Trans. Ind. Electron.*, vol. 61, no. 5, pp. 2197–2207, May 2014.

[45] E. Levi, D. Dujic, M. Jones, and G. Grandi, "Analytical determination of dc-bus utilization limits in multiphase VSI supplied ac drives," *IEEE Trans. Energy Convers.*, vol. 23, no. 2, pp. 433–443, Jun. 2008.

[46] T. Nishijima, M. Tanaka, A. Imayanagita, Y. F. Chen, K. Fujikawa, and H. Kobayashi, "Direct instantaneous harmonic distortion minimization control for three phase sinusoidal current converter," in *Proc. 29th Annu. IEEE Power Electron. Spec. Conf.*, 1998, pp. 510–516.

[47] J. Loncarski, "Peak-to-peak output current ripple analysis in multiphase and multilevel inverters," Ph.D. thesis, Dept. Electr. Eng., Bologna Univ., Bologna, Italy, 2014.

[48] P. A. Dahono, Deni, and E. G. Supriatna, "Output current-ripple analysis of five-phase PWM inverters," *IEEE Trans. Ind. Appl.*, vol. 45, no. 6, pp. 2022–2029, Nov./Dec. 2009.

[49] D. Dujic, M. Jones, E. Levi, J. Prieto, and F. Barrero, "Switching ripple characteristics of space vector PWM schemes for five-phase two-level voltage source inverters—Part 1: Flux harmonic distortion factors," *IEEE Trans. Ind. Electron.*, vol. 58, no. 7, pp. 2789–2798, Jul. 2011.

[50] M. Jones, D. Dujic, E. Levi, J. Prieto, and F. Barrero, "Switching ripple characteristics of space vector PWM schemes for five-phase two-level voltage source inverters—Part 2: Current ripple," *IEEE Trans. Ind. Electron.*, vol. 58, no. 7, pp. 2799–2808, Jul. 2011.
[51] X. Wu, G. Tan, Z. Ye, Y. Liu, and S. Xu, "Optimized common-mode voltage reduction PWM for three-phase voltage-source inverters," *IEEE Trans. Power Electron.*, vol. 31, no. 4, pp. 2959–2969, Apr. 2016.
[52] A. Lewicki, "Dead-time effect compensation based on additional phase current measurements," *IEEE Trans. Ind. Electron.*, vol. 62, no. 7, pp. 4078–4085, Jul. 2015.

Wenjing Xiong was born in Hunan, China, in 1991. She received the B.S. degree in automation, in 2012, from the Central South University, Changsha, China, where she is currently working toward the Ph.D. degree in electrical engineering.

Her research interests include matrix converter, ac/dc converter, and solid state transformer.

Yao Sun (M'13) was born in Hunan, China, in 1981. He received the B.S. degrees in automation, and the M.S., and Ph.D. degrees in electric engineering from the School of Information Science and Engineering, Central South University, Changsha, China, in 2004, 2007, and 2010, respectively.

Since 2013, he has been an Associate Professor in the School of Information Science and Engineering, Central South University. His research interests include matrix converter, microgrid, and wind energy conversion system.

Mei Su was born in Hunan, China, in 1967. She received the B.S. in automation, M.S., and Ph.D. degrees in electric engineering from the School of Information Science and Engineering, Central South University, Changsha, China, in 1989, 1992, and 2005, respectively.

Since 2006, she has been a Professor in the School of Information Science and Engineering, Central South University. Her research interests include matrix converter, adjustable speed drives, and wind energy conversion system.

Jianxin Zhang was born in Shandong, China, in 1992. He received the B.S. degree in electrical engineering from the Central South University, Changsha, China, in 2015, where he is currently working toward the M.S. degree.

His research interests include matrix converter and wireless power transmission.

Yonglu Liu was born in Chongqing, China, in 1989. He received the B.S. and M.S. degrees in electrical engineering from the Central South University, Changsha, China, in 2012 and 2015, respectively. He is currently working toward the Ph.D. degree in electrical engineering.

His research interests include matrix converter and ac/dc converter.

Jian Yang (M'09) received the Ph.D. degree in electrical engineering from the University of Central Florida, Orlando, FL, USA, in 2008.

He was a Senior Electrical Engineer with Delta Tau Data Systems, Inc., Los Angeles, CA, from 2007 to 2010. Since 2011, he has been with the Central South University, Changsha, China, where he is currently an Associate Professor in the School of Information Science and Engineering. His main research interests include control application, motion planning, and power electronics.